catalysts

MDPI

Article

A Theoretical Insight into Enhanced Catalytic Activity of Au by Multiple Twin Nanoparticles

Kyoichi Sawabe [1,*], Taiki Koketsu [1], Junya Ohyama [1,2] and Atsushi Satsuma [1,2]

[1] Graduate School of Engineering, Nagoya University, Nagoya, Aichi 464-8603, Japan; kouketsu.taiki@a.mbox.nagoya-u.ac.jp (T.K.); ohyama@chembio.nagoya-u.ac.jp (J.O.); satsuma@chembio.nagoya-u.ac.jp (A.S.)

[2] ESICB, Kyoto University, Katsura, Kyoto 615-8520, Japan

* Correspondence: sawabe@chembio.nagoya-u.ac.jp; Tel.: +81-52-789-2610

Academic Editor: José R. B. Gomes

Received: 15 May 2017; Accepted: 16 June 2017; Published: 19 June 2017

Abstract: Recently, it has been reported that the morphology of Au nanoparticles (NPs) affects the catalytic activity of CO oxidation; twin crystal NPs show higher activity for CO oxidation than single-crystal NPs. In this study, density functional calculations have been carried out to investigate the morphology effect of Au NPs using CO as a probe molecule. In the case of Au NPs with a size of more than 2 nm, CO adsorption energy on the Au NPs is mainly determined by a coordination number (CN) of adsorption sites. CO binding to a multiple twin NP with a size of about 1 nm is stronger than that on a single-crystal NP with the same size. A simple CN explanation cannot be applied to the enhancement of CO binding to the small multiple twin NP. This enhancement is related to a deformation of the NP structure before and after CO adsorption. It is suggested that the multiple twin NP with a size of less than 1 nm, which shows the deformation upon CO adsorption, contributes to the higher activity for CO oxidation.

Keywords: Au nanoparticles; twin; CO oxidation; density functional theory

1. Introduction

It is well known that gold nanoparticles (NPs) show high catalytic activity for CO oxidation at low temperature [1–3]. The catalytic activity is affected by the size of Au NPs and abruptly increases as its size decreases to less than 3 nm. The size effect is sometimes explained by the reactivity in terms of special reaction sites at the metal–support interface [2,4]. There is another explanation for the size effect [5–7]. The percentage of highly-uncoordinated gold atoms on the Au NP surface yields observed differences in the reactivity of Au NPs. Other than the size, the morphology of Au NPs also influences their catalysis [8–16]. The ratio of different surface facets depends not only on the size of the nanoparticles, but also their morphology [17]. The morphology, which determines the number of coordination sites available, such as corners and edges, is also important for the catalytic activity. For example, the activity of the water-gas shift (WGS) reaction over Au/CeO_2 drastically decreased with the loss of the 2D-layer morphology of Au [12]. Choudhary et al. suggested that quantum size effects, as a result of bilayered Au morphology, were important [8]. However, there is controversy regarding the explanation of the activity based on the thickness of the Au morphology. Lemire et al. [6] studied CO adsorption on gold monolayer islands and found that the adsorption property was no different from that on bulk gold. They suggested that the exceptional activity of gold nanoparticles for the low-temperature CO oxidation arose from the presence of highly-uncoordinated atoms. Twinning of Au NPs shows higher activity for the CO oxidation reaction than single crystal Au NPs [9,14,15]. The morphology effect by twinning was shown to be independent of the size effect. Even though Au NPs with the same particle distribution were synthesized, twin NPs were more active for CO oxidation

than single-crystal NPs [14]. Determining the reason why twin NPs are more active will give us a deeper understanding for the design of Au NP catalyst.

In this study, density functional calculations have been carried out to investigate the morphology effect of Au NPs using CO as a probe molecule. This is because CO adsorption has been reported to have a strong correlation with the catalytic activity for CO oxidation [18–20]. The morphology effect of NPs ranging from 1 to 3 nm in size is examined. The morphology effect for NPs ranging from 2 to 3 nm in size can be explained by the coordination number of adsorption sites. For five-fold twin NPs with a size of 1 nm, the stability of NPs upon CO adsorption affects CO adsorption energy on the NP. Thus, the stability of NPs upon CO adsorption is also significant for the morphology effect.

2. Computational Details

Spin-polarized density-functional theory (DFT) calculations were performed using the plane wave self consistent field (PWscf) code in Quantum Espresso [21]. We employed the Perdew–Burke–Ernzerhof (PBE) exchange correlation functional [22,23] and Vanderbilt ultra-pseudopotentials [24]. The system wave function was represented by a basis set of plane waves limited by an energy cutoff of 30 Ry, while the cutoff for the electron density representation was set to 300 Ry (1 Ryd $\approx$ 13.6 eV). All geometry optimizations were performed until the maximum force on atoms was less than 10^{-3} au. A cubic unit cell of 34 $\times$ 34 $\times$ 34 Å was used for large NPs and a unit of 21 $\times$ 21 $\times$ 21 Å was used for the smallest NPs and an isolated CO molecule. The sizes of the unit cells were sufficient to electronically isolate periodic images of the nanoparticles. A gamma k-point sampling of the Brillouin zone was chosen. Adequate spin states of nanoparticles were assigned using total magnetization parameters. The Fermi-Dirac smearing procedure [25] with a smearing parameter of 0.0007 Ry was applied. This smearing width is sufficiently small to gurantee a correct description of the spin states [26]. CO adsorption energy (E_{ad}) on NPs was calculated using the following equation:

$$E_{ad} = E(\text{CO-NP}) - E(\text{NP}) - E(\text{CO}) \quad (1)$$

Here, E(CO-NP) is the total energy of the Au NP interacting with CO, E(NP) is the total energy of the Au NP without CO, and E(CO) is the energy of the isolated CO molecule. Thus, a negative value of E_{ad} means an exothermic adsorption.

The point group symmetry determined by the morphology of the NP affects the electronic states in the whole system. In the case of small Au clusters, the spin states do not always have the lowest spin because the high symmetry of Au clusters has a possibility of exhibiting degenerate states at the higest occupied molecular orbital level [26]. For example, a small Ag cluster with a symmetry of I_h has high spin states [27]. Symmetry change by the morphology is also important for the interpretation of observed spectra [28]. We calculated several spin states for Au_{55} NPs with a high symmetry of O_h. For the sake of comparison, the same spin states were calculated at the M06L/Def2-TZVPP(SDD)//M06L/Def2-SVP(SDD) level using the ORCA code [29]. Table 1 shows the results. The ground state of Au_{55} NP has the spin state of S_z = 0 and the energy difference to the first excited state is large. The lowest spin state is also expected for the large size of NPs with a lower symmetry than O_h. All spin states of Au NPs in this study were assumed to have the lowest spin. That is to say, the z component of the spin, S_z, was equal to 0 for even numbers of atoms and 1/2 for odd numbers of atoms.

Table 1. Energy in eV of Au_{55} (O_h) relative to that of the spin state of S_z = 0.

S_z	PBE/Plane Wave	M06L/Def2-TZVPP(SDD) *
1/2	-	-
3/2	0.26	0.25
5/2	1.00	0.99

* Geometry optimizations were carried out at the M06L/Def2-SVP(SDD) level.

3. Results

3.1. Model Nanoparticles

Figure 1 shows examples of the morphology of NPs adopted in this study. A truncated cuboctahedron structure is used for a single-crystal nanoparticle. This structure has a symmetry of O_h. Hereafter, we call the single-crystal NP as "O_h-NP". In the O_h-NP structure, (111) faces are always located next to (100) faces. For twin NPs, two types of structures are adopted; one is a single twin structure, which has a single grain boundary, and the other is a multiple twin type, which has five-fold twinning. Both types of twin NPs were experimentally observed [13,14]. The single-twin NP has the symmetry of D_{3h} (hereafter, referred to as "D_{3h}-NP"). In the D_{3h}-NP structure, the single twinning results in the grain boundary at which the (111) and (100) faces are next to the (111) and (100) faces, respectively. The five-fold twin NP is a decahedron and has the symmetry of D_{5h} (hereafter, referred to as "D_{5h}-NP"). The D_{5h}-NP is composed of five distorted tetrahedral units, which are joined at a common edge and each of which shares two of their (111) faces as twinning planes.

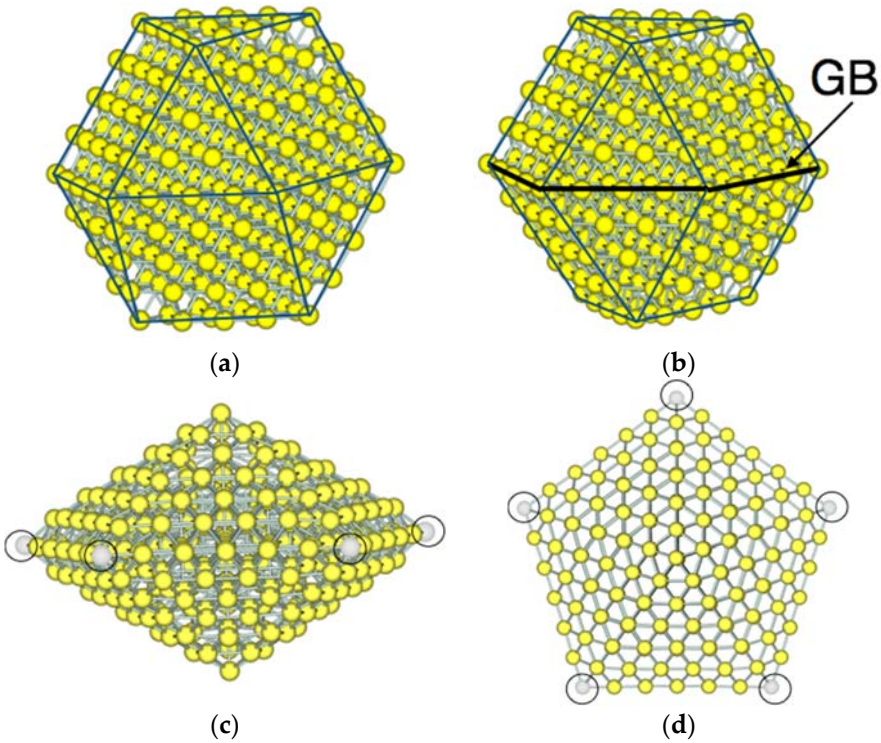

Figure 1. Morphology of model Au nanoparticles (NPs). (**a**) A single-crystal structure with the symmetry of O_h (O_h-NP). The (100) faces depicted by a rectangle are always next to the (111) faces depicted by a triangle; (**b**) a single twin structure with the symmetry of D_{3h} (D_{3h}-NP) which has a grain boundary (GB). At the grain boundary, the (100) and (111) faces are always next to the (100) and (111) faces, respectively; (**c**) side view and (**d**) top view of the multiple twin structure with the symmetry of D_{5h} (D_{5h}-NP). This structure exhibits five-fold twinning which share the neighboring (111) faces.

To investigate the size dependency of CO adsorption, several sizes of NPs were created, as shown in Figure 2. The smallest size of NP is Au_{55} for the O_h-NP and D_{3h}-NP. The size of NP is increased by adding atoms all around the particle. We categorized three generations of different sizes of NP for both structures. As shown in Figure 2a,b, the first generation is Au_{55} NPs which have a diameter of about 1 nm. The second generation and the third generation are Au_{147} with a diameter of about 2 nm and Au_{309} with a diameter of about 3 nm, respectively. In the case of the D_{5h}-NP, the size is increased by alternately adding atoms to the upper side and lower side of the particle. As a result, the spin states change with the increase in NP size because the number of atoms varies to be even and odd,

alternatively. To hold the same symmetry and spin state, five atoms at corners (white atoms marked by black circles in Figure 1c,d) are used for adjuster atoms. For example, the removal of the five atoms from Au_{54} with the spin state of $S_z = 0$ leads to the D_{5h}-NP of Au_{49} which has the spin state of $S_z = 1/2$ with the same D_{5h} symmetry. Although the removal of these atoms elongates a bond length between an atom at a vertex adsorption site and the neighboring atoms by 0.04 Å (2.79 Å to 2.82 Å), the shape around the adsorption sites remains the same. For the D_{5h}-NP of $S_z = 1/2$, Au_{49} is the first generation, with a diameter of about 1 nm. Au_{105} and Au_{181} are the second generation, which have a diameter of about 2 nm. Au_{287} is the third generation, with a diameter of about 3 nm. In the case of the spin state of $S_z = 0$, the five corner atoms (white atoms in Figure 1c,d) in the second and third generations of NPs are removed to make the number of atoms even.

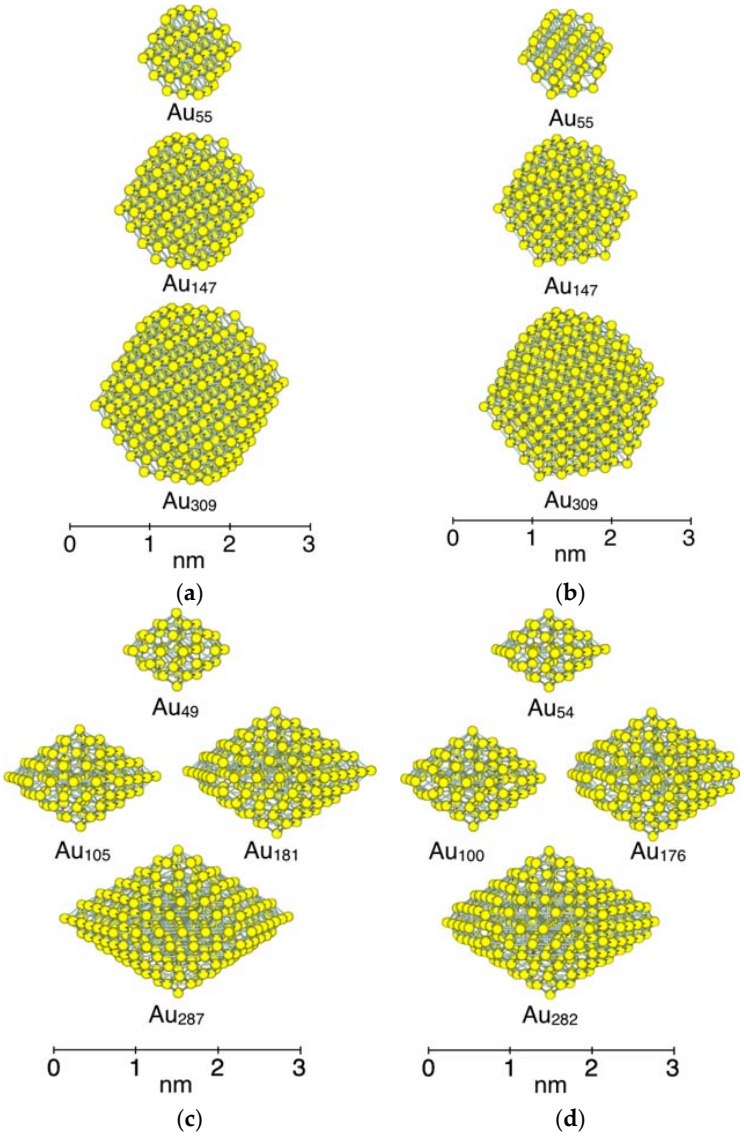

Figure 2. Size of model Au NPs. (**a**) Single-crystal O_h-NPs; (**b**) simple twin D_{3h}-NPs; (**c**) multiple twin D_{5h}-NPs with the spin state of $S_z = 1/2$; and (**d**) multiple twin D_{5h}-NPs with the spin state of $S_z = 0$. Three generations are categorized for these NPs. The first generation includes NPs of less than 100 atoms and their diameters are about 1 nm. The second generation includes NPs composed of 100 to 200 atoms and their diameters are about 2 nm. The third generation includes NPs of around 300 atoms, and their diameters are about 3 nm.

Figure 3 shows the adsorption sites on Au NPs; vertex sites in Figure 3a, edge sites in Figure 3b, and face sites in Figure 3c. For the single-twin NP, the vertex site at the grain boundary was examined. Two types of face sites are shown for the O_h-NP, which has (100) and (111) faces. There is a possibility of a bridge and three-fold-type adsorption on these faces. In our calculation, bridge-type adsorption on the (111) face yielded more stable adsorption than on-top adsorption. When interaction between co-adsorbed molecules can be neglected, multiple bonds between a molecule and surface atoms give rise to more stable adsorption than a single bond. Thus, the bridge-type adsorption for a single molecule, in general, yields a more stable adsorption than the on-top adsorption. Since the objective of this study is to compare the CO adsorption by varying the size and the morphology of NPs, adsorption sites are limited to the on-top adsorption.

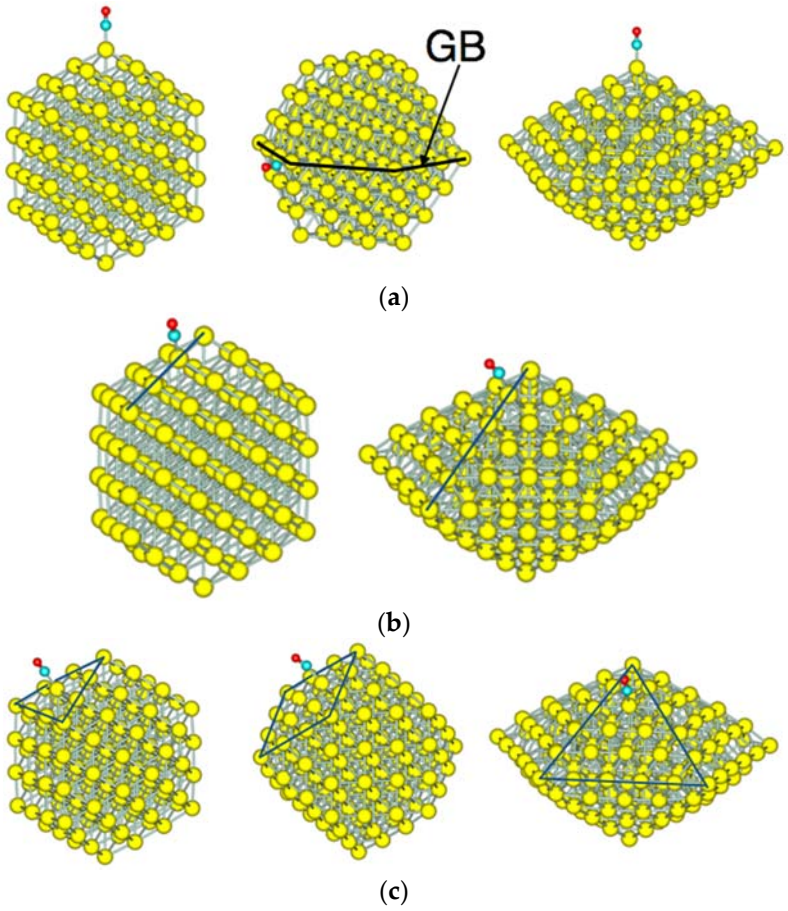

Figure 3. CO adsorption sites of NPs. All adsorption sites are the on-top type. (**a**) Vertex sites of the O_h-NP, D_{3h}-NP, and D_{5h}-NP. On the D_{3h}-NP, the vertex site is located at the grain boundary (GB); (**b**) edge sites of the O_h-NP and D_{5h}-NP; and (**c**) face sites of the O_h-NP and D_{5h}-NP. The O_h-NP has both the (111) face (left) and the (100) face (middle). The D_{5h}-NP has only the (111) face. Yellow, cyan, and red spheres represent Au, C, and O atoms, respectively.

3.2. Size Dependency of CO Adsoprtion

Figure 4 shows the plot of the CO adsorption energy on the vertex sites as a function of the number of Au atoms. For the O_h-NP and D_{3h}-NP, CO adsorption strength gradually decreases as the increase of the number of Au atoms. The differences in energy between the size of about 1 nm and 3 nm are 0.04 eV for the O_h-NP and 0.03 eV for the D_{3h}-NP. Thus, the adsorption energy is mainly determined by the local environment of the adsorption sites, such as the coordination number (CN). The CN of the adsorption sites is a good descriptor for the CO binding to Au NPs [7,19]. Since the CN

of the vertex sites of the O_h-NP and D_{3h}-NPs is equal to five, CO adsorption energies of the O_h-NP differ slightly from those of the single-twin NP in all sizes. For the second and the third generations, the D_{5h}-NPs show weaker binding than the O_h-NPs. This is also explained by the coordination number. The CN for the D_{5h}-NP is six, whereas that for the O_h-NP is five. Therefore, the more unsaturated site of the O_h-NP results in the more stable adsorption of CO. The exception occurs in the case of the first generation of the D_{5h}-NP.

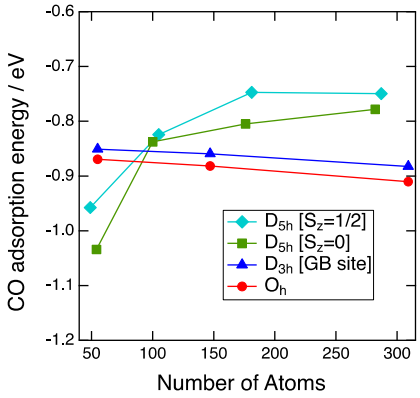

Figure 4. CO adsorption energy on the vertex sites plotted with respect to the number of atoms of NPs. Aqua diamonds, green squares, blue triangles, and red circles represent the CO adsorption energies on the D_{5h}-NPs with spin states of $S_z = 1/2$, the D_{5h}-NPs with spin states of $S_z = 0$, the D_{3h}-NPs and the O_h-NPs, respectively.

The size dependence of the CO adsorption energy for the D_{5h}-NPs is reverse to that of the O_h-NP. Furthermore, the energy abruptly decreases from the second to the first generation and the CO adsorption on the D_{5h}-NP becomes more stable than that of the O_h-NP. This stabilization cannot be explained by the simple CN consideration. This is not due to the strain effect because the local structure around the adsorption sites is not affected by the morphology or the size. The average bond distance between a site atom and the neighboring atoms is 2.82 Å for the D_{5h}-Au_{54}, 2.83 Å for the D_{5h}-Au_{282}, and 2.84 Å for the O_h-Au_{309}. The small difference between these values indicates no strain effect. Next, we focused on the deformation of NPs before and after CO adsorption, since CO adsorption leads to the structural change of the NP itself. Root-mean-square distances (RMSD) between atom positions of NPs were used as a quantitative index for the structural change. At first, the local deformation around the adsorption sites was examined. The average RMSD of the site and neighboring atoms for the D_{5h}-NP (Au_{54}, $S_z = 0$) and O_h-NP (Au_{55}) were 6.9 pm and 6.8 pm, respectively. Thus, the local changes of both NPs induced by CO adsorption are almost the same. Next, the deformation of the whole NP structure was examined. The average RMSD of all atoms for the D_{5h}-NP (Au_{54}, $S_z = 0$) and O_h-NP (Au_{55}) were 13.9 pm and 3.1 pm, respectively. The average RMSD increased for the D_{5h}-NP and decreased for the O_h-NP. This means that CO adsorption on the D_{5h}-NP results in the structural change of all of the NP atoms, whereas that on the O_h-NP only affects the local structure around the adsorption sites. Partial optimizations of CO adsorption on the D_{5h}-NPs of Au_{54} and Au_{49} with fixing NP geometries led to the adsorption energies of -0.76 eV and -0.84 eV, respectively. Adsorption energies by the full optimizations were -1.03 eV and -0.96 eV for Au_{54} and Au_{49}, respectively. Thus, the stabilization by deformation was 0.27 eV for Au_{54} and 0.12 eV for Au_{49}. The average RMSD for the D_{5h}-NPs of Au_{54} and Au_{49} were 13.9 pm and 7.2 pm. Thus, the stabilization is related to the deformation degree of the whole NP structure upon CO adsorption. In other words, the morphology effect of the multiple twin NP around the size of about 1 nm arises from the stability of the whole NP structure upon CO adsorption.

3.3. CO Adsorption vs. the Coordination Number

As shown in Figure 4, the size dependence on the CO adsorption for the D_{5h}-NP and O_h-NP with the same spin state of $S_z = 1/2$ is small between the second and third generations. Therefore, the pure CN dependence without the size effect can be estimated. We calculated the predicted adsorption energy of the O_h-NP of Au_{287}, which had the same number of atoms as the largest D_{5h}-NP, using an interpolation method. Figure 5 shows the plot of the CO adsorption energy as a function of the CN of the on-top sites. Adsorption energies at CN 5, 6, 7, and 9 were obtained from the adsorptions on the vertex site of the O_h-NP, the vertex of the D_{5h}-NP, the edge of the O_h-NP, and the (111) face of the O_h-NP, respectively. Energies at CN 8 were calculated from the adsorption on the edge site of the D_{5h}-NP and the (100) face sites of the O_h-NP. We can clearly establish a linear relationship between the CN and the CO adsorption energy as:

$$E_{ad}/eV = 0.14 \times CN - 1.61. \quad (2)$$

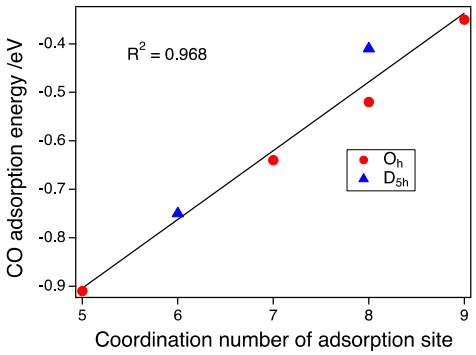

Figure 5. CO adsorption energy as a function of the coordination number of adsorption sites. Red circles and blue triangles represent the CO adsorption energies on the O_h-NPs and D_{5h}-NPs ($S_z = \frac{1}{2}$), respectively.

The CO binding dependence on the CN has been already reported [19,30]. Mpourmpakis et al. used bond angles plus the CN as parameters for fitting. The need for bond angles is because they include the size and shape effect into such parameters. The absolute values reported by Lopez et al. [19] are different from our results. The adsorption energy in our study is the expected value in the case of the bulk surface because the size of NPs in our study is large enough to suppress the deformation upon CO adsorption. Experimentally, CO adsorption energies on an Au(211) surface, or 3(111) × (100) in microfacet notation, was determined [31]. The adsorption energy on a step-like (100) facet was 0.52 eV. The adsorption energy on a (111) face was estimated to be −0.28 to −0.39 eV. These experimental values agree with our calculated values. Since the energy dependence on the size is small for the large NPs with a size of more than 2 nm, the adsorption strength can be determined by the CN of the adsorption sites alone. Thus, the morphology effect of such large NPs can be explained by the number of CNs in the surface atoms [7].

4. Discussion

Now, we discuss the catalytic activity of the multiple twin Au-NP. The enhanced binding of CO for Au NPs is central to understanding the enhanced catalytic properties. Meier and Goodman observed the heat of CO adsorption for Au NPs ranging in size from 1.8 to 3.1 nm. They showed that the size of Au NP with the highest heat was very close to that exhibiting the maximum catalytic activity for CO oxidation [20]. DFT works by Lopez et al. [19] and Hvolbæk et al. [32] reported that the coordination number (CN) was the important factor for CO oxidation over Au catalysts in comparison to the role of charge transfer, layer thickness, and interactions with the support. Taylor et al. [7] reported that the relation between the CO oxidation activity and the average CO binding energy was

affected by the average surface CN. In the case of the O_h-NPs in our study, the average surface CN was 7.2 for Au_{147} to 6.6 for Au_{55}. According to Equation (2), the decrease in size leads to the increase in CO binding by 0.84 eV. Thus, the size effect for catalytic activity using the CN can be applied for the O_h-NP. For the second and third generations, this estimate is also applicable for the D_{5h}-NP, which had the average surface CN of more than 7.4 (see Table S1). Since CO binding on the D_{5h}-NP was weak, the D_{5h}-NPs of this size are not active species for enhanced CO oxidation. On the other hand, the CO adsorption energy of the D_{5h}-NP in the first generation was more negative than that of the O_h-NP. Thus, the species showing higher catalytic activity than the single-crystal NPs are expected to be multiple twin structures with a size of less than 1 nm. The enhancement comes from the deformation of the whole NP structure, or the stability of Au-NP, upon gas adsorption. Some theoretical studies [33,34] reported the relation between the stability of metal NPs upon gas adsorption and the activity for CO oxidation. Recently, environmental transmission electron microcopy (ETEM) measurement showed that the fraction of morphology-changeable Au-NPs is not negligible for catalytic activity [35].

Finally, we suggest a ratio of surface atoms as a simple descriptor of the deformation effect mentioned above. Figure 6 shows the plot of the average RMSD for the vertex adsorption of all NPs as a function of the ratio of surface atoms to all atoms of the NPs. When the ratio of the surface atoms was 0.8 or more, the deformation described by the average RMSD increased sharply. Although this deformation occurred only for the multiple twin NPs (D_{5h}-NPs) in our case, this would also occur for NPs that have a symmetry other than D_{5h} in the case of the smaller size of NPs. Since the average RMSD represents the stability of Au NP upon CO adsorption, there is a possibility that the ratio of surface atoms can be a reaction descriptor for small NPs, in which the stability is significant for gas adsorption.

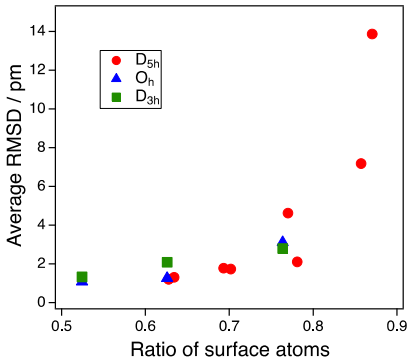

Figure 6. Average RMSD as a function of the ratio of surface atoms. Average RMSD represents an average value of the root mean square distances (RMSDs) of all NP atom coordinates before and after CO adsorption.

5. Conclusions

DFT calculations were performed for CO adsorption on three generations of Au NPs with sizes of about 1, 2, and 3 nm. The size effect for the CO adsorption energy on the vertex site was small in the case of the single-crystal structure and the single-twin structure. For NPs larger than 2 nm, the CO adsorption energy was mainly determined by the coordination number of the adsorption sites, regardless of the symmetry of the Au NPs. Under the condition that the size effect was removed, a clear linear relationship between the adsorption energy and the coordination number (CN) was obtained without another parameter, such as bond angles. The size dependence of CO adsorption on the vertex site for the multiple twin structure of D_{5h} was large, and a sharp enhancement occurred as the size decreased from 2 nm to 1 nm. This was not due to the strain effect. The deformation of the whole NP structure before and after CO adsorption was large for the multiple twin structure with a size of 1 nm. This deformation resulted in the enhancement of CO adsorption on the multiple twin NP. Thus, the morphology effect for the small size of multiple twin NPs arises from the deformation

upon CO adsorption. Finally, we suggested a ratio of surface atoms as a simple descriptor for the deformation effect. When the ratio of the surface atoms was 0.8 or more, the deformation described by the average RMSD increased sharply. In such cases, the CO adsorption energy must be estimated by the deformation in addition to the CN.

Supplementary Materials: The following is available online at www.mdpi.com/2073-4344/7/6/191/s1, Table S1: CO adsorption energy, average surface CN, ratio of surface atoms, and average RMSD for all Au NPs.

Acknowledgments: This work was supported by JSPS KAKENHI Grant-in-Aid for Young Scientists (A), No. 16H06131. The computations were performed at the Research Center for Computational Science, Okazaki, Japan.

Author Contributions: K.S. conceived the computational study, based on higher-level discussions of Au twin-particle with J.O. and A.S. K.S. performed the simulation and analysis, with Au NP structures for input from T.K. K.S. wrote the paper. All authors contributed to preparing the manuscript.

Conflicts of Interest: The authors declare no conflict of interest.

References

1. Haruta, M. Chance and necessity: My encounter with gold catalysts. *Angew. Chem. Int. Ed. Engl.* **2014**, *53*, 52–56. [CrossRef] [PubMed]
2. Ishida, T.; Koga, H.; Okumura, M.; Haruta, M. Advances in Gold Catalysis and Understanding the Catalytic Mechanism. *Chem. Rec.* **2016**, *16*, 2278–2293. [CrossRef] [PubMed]
3. Min, B.K.; Friend, C.M. Heterogeneous gold-based catalysis for green chemistry: Low-temperature CO oxidation and propene oxidation. *Chem. Rev.* **2007**, *107*, 2709–2724. [CrossRef] [PubMed]
4. Fujita, T.; Tokunaga, T.; Zhang, L.; Li, D.W.; Chen, L.Y.; Arai, S.; Yamamoto, Y.; Hirata, A.; Tanaka, N.; Ding, Y.; et al. Atomic Observation of Catalysis-Induced Nanopore Coarsening of Nanoporous Gold. *Nano Lett.* **2014**, *14*, 1172–1177. [CrossRef] [PubMed]
5. Brodersen, S.H.; Grønbjerg, U.; Hvolbæk, B.; Schiøtz, J. Understanding the catalytic activity of gold nanoparticles through multi-scale simulations. *J. Catal.* **2011**, *284*, 34–41. [CrossRef]
6. Lemire, C.; Meyer, R.; Shaikhutdinov, S.; Freund, H.J. Do quantum size effects control CO adsorption on gold nanoparticles? *Angew. Chem. Int. Ed. Engl.* **2004**, *43*, 118–121. [CrossRef] [PubMed]
7. Taylor, M.G.; Austin, N.; Gounaris, C.E.; Mpourmpakis, G. Catalyst Design Based on Morphology- and Environment-Dependent Adsorption on Metal Nanoparticles. *ACS Catal.* **2015**, *5*, 6296–6301. [CrossRef]
8. Choudhary, T.V.; Goodman, D.W. Catalytically active gold: The role of cluster morphology. *Appl. Catal. A Gen.* **2005**, *291*, 32–36. [CrossRef]
9. Cunningham, D.A.H.; Vogel, W.; Sanchez, R.M.T.; Tanaka, K.; Haruta, M. Structural analysis of Au/TiO_2 catalysts by Debye function analysis. *J. Catal.* **1999**, *183*, 24–31. [CrossRef]
10. Feng, X.F.; Jiang, K.L.; Fan, S.S.; Kanan, M.W. Grain-Boundary-Dependent CO_2 Electroreduction Activity. *J. Am. Chem. Soc.* **2015**, *137*, 4606–4609. [CrossRef] [PubMed]
11. Kartusch, C.; Krumeich, F.; Safonova, O.; Hartfelder, U.; Makosch, M.; Sa, J.; van Bokhoven, J.A. Redispersion of Gold Multiple Twinned Particles during Liquid-Phase Hydrogenation. *ACS Catal.* **2012**, *2*, 1394–1403. [CrossRef]
12. Lin, Y.; Wu, Z.; Wen, J.; Ding, K.; Yang, X.; Poeppelmeier, K.R.; Marks, L.D. Adhesion and Atomic Structures of Gold on Ceria Nanostructures: The Role of Surface Structure and Oxidation State of Ceria Supports. *Nano Lett.* **2015**, *15*, 5375–5381. [CrossRef] [PubMed]
13. Mohr, C.; Hofmeister, H.; Claus, P. The influence of real structure of gold catalysts in the partial hydrogenation of acrolein. *J. Catal.* **2003**, *213*, 86–94. [CrossRef]
14. Ohyama, J.; Koketsu, T.; Yamamoto, Y.; Arai, S.; Satsuma, A. Preparation of TiO_2-supported twinned gold nanoparticles by CO treatment and their CO oxidation activity. *Chem. Commun.* **2015**, *51*, 15823–15826. [CrossRef] [PubMed]
15. Pandey, A.D.; Guttel, R.; Leoni, M.; Schuth, F.; Weidenthaler, C. Influence of the Microstructure of Gold-Zirconia Yolk-Shell Catalysts on the CO Oxidation Activity. *J. Phys. Chem. C* **2010**, *114*, 19386–19394. [CrossRef]

16. Quintanilla, A.; Butselaar-Orthlieb, V.C.L.; Kwakernaak, C.; Sloof, W.G.; Kreutzer, M.T.; Kapteijn, F. Weakly bound capping agents on gold nanoparticles in catalysis: Surface poison? *J. Catal.* **2010**, *271*, 104–114. [CrossRef]
17. Marks, L. Experimental studies of small particle structures. *Rep. Prog. Phys.* **1994**, *57*, 603. [CrossRef]
18. Falsig, H.; Hvolbæk, B.; Kristensen, I.S.; Jiang, T.; Bligaard, T.; Christensen, C.H.; Nørskov, J.K. Trends in the catalytic CO oxidation activity of nanoparticles. *Angew. Chem.* **2008**, *120*, 4913–4917. [CrossRef]
19. Lopez, N.; Janssens, T.V.W.; Clausen, B.S.; Xu, Y.; Mavrikakis, M.; Bligaard, T.; Nørskov, J.K. On the origin of the catalytic activity of gold nanoparticles for low-temperature CO oxidation. *J. Catal.* **2004**, *223*, 232–235. [CrossRef]
20. Meier, D.C.; Goodman, D.W. The influence of metal cluster size on adsorption energies: CO adsorbed on Au clusters supported on TiO(2). *J. Am. Chem. Soc.* **2004**, *126*, 1892–1899. [CrossRef] [PubMed]
21. Giannozzi, P.; Baroni, S.; Bonini, N.; Calandra, M.; Car, R.; Cavazzoni, C.; Ceresoli, D.; Chiarotti, G.L.; Cococcioni, M.; Dabo, I.; et al. QUANTUM ESPRESSO: A modular and open-source software project for quantum simulations of materials. *J. Phys. Condens. Matter* **2009**, *21*, 395502. [CrossRef] [PubMed]
22. Perdew, J.P.; Burke, K.; Ernzerhof, M. Generalized gradient approximation made simple. *Phys. Rev. Lett.* **1996**, *77*, 3865. [CrossRef] [PubMed]
23. Perdew, J.P.; Burke, K.; Ernzerhof, M. Generalized Gradient Approximation Made Simple [Phys. Rev. Lett. 77, 3865 (1996)]. *Phys. Rev. Lett.* **1997**, *78*, 1396. [CrossRef]
24. Vanderbilt, D. Soft self-consistent pseudopotentials in a generalized eigenvalue formalism. *Phys. Rev. B* **1990**, *41*, 7892–7895. [CrossRef]
25. Methfessel, M.; Paxton, A.T. High-precision sampling for Brillouin-zone integration in metals. *Phys. Rev. B* **1989**, *40*, 3616–3621. [CrossRef]
26. Gruber, M.; Heimel, G.; Romaner, L.; Brédas, J.-L.; Zojer, E. First-principles study of the geometric and electronic structure of Au13 clusters: Importance of the prism motif. *Phys. Rev. B* **2008**, *77*, 165411. [CrossRef]
27. Pereiro, M.; Baldomir, D.; Arias, J.E. Unexpected magnetism of small silver clusters. *Phys. Rev. A* **2007**, *75*, 063204. [CrossRef]
28. Sawabe, K.; Hiro, T.; Shimizu, K.-i.; Satsuma, A. Density functional theory calculation on the promotion effect of H2 in the selective catalytic reduction of NOx over Ag–MFI zeolite. *Catal. Today* **2010**, *153*, 90–94. [CrossRef]
29. Neese, F. The ORCA program system. *Wiley Interdiscip. Rev. Comput. Mol. Sci.* **2012**, *2*, 73–78. [CrossRef]
30. Mpourmpakis, G.; Andriotis, A.N.; Vlachos, D.G. Identification of descriptors for the CO interaction with metal nanoparticles. *Nano Lett.* **2010**, *10*, 1041–1045. [CrossRef] [PubMed]
31. Kim, J.; Samano, E.; Koel, B.E. CO adsorption and reaction on clean and oxygen-covered Au(211) surfaces. *J. Phys. Chem. B* **2006**, *110*, 17512–17517. [CrossRef] [PubMed]
32. Hvolbæk, B.; Janssens, T.V.W.; Clausen, B.S.; Falsig, H.; Christensen, C.H.; Nørskov, J.K. Catalytic activity of Au nanoparticles. *Nano Today* **2007**, *2*, 14–18. [CrossRef]
33. Shimizu, K.-i.; Sawabe, K.; Satsuma, A. Self-Regenerative Silver Nanocluster Catalyst for CO Oxidation. *ChemCatChem* **2011**, *3*, 1290–1293. [CrossRef]
34. Zhang, W.; Cheng, D.; Zhu, J. Theoretical study of CO catalytic oxidation on free and defective graphene-supported Au–Pd bimetallic clusters. *RSC Adv.* **2014**, *4*, 42554–42561. [CrossRef]
35. Uchiyama, T.; Yoshida, H.; Kamiuchi, N. Correlation of catalytic activity with the morphology change of supported Au nanoparticles in gas. *Surf. Sci.* **2017**, *659*, 16–19. [CrossRef]